Positively-charged, porous, polysaccharide nanoparticles loaded with anionic molecules behave as 'stealth' cationic nanocarriers.

Archibald Paillard, Catherine Passirani, Patrick Saulnier, Maya Kroubi, Emmanuel Garcion, Jean-Pierre Benoît, Didier Betbeder

Positively-charged, porous, polysaccharide nanoparticles loaded with anionic molecules behave as 'stealth' cationic nanocarriers

Archibald Paillard [a], Catherine Passirani [a #], Patrick Saulnier [a], Maya Kroubi [b], Emmanuel Garcion [a], Jean-Pierre Benoît [a], Didier Betbeder [b, c]

[a] *INSERM U646 Ingénierie de la vectorisation particulaire; Université d'Angers, 10 rue André Boquel, Angers 49100, France*

[b] *EA 2689, IFR 114 laboratoire de physiologie; Université de Lille 2, 1 place de verdun, Lille 59045 cedex, France*

[c] *Université d'Artois, Rue Jean Souvraz, Lens 62307 France*

[#] Corresponding author: Catherine Passirani : Institut National de la Santé et de la Recherche Médicale, Inserm U646 ; 10 rue André Boquel, 49100 Angers, France. Tél. : 33 (0)2 41 73 58 50 –Fax : 33 (0)2 41 73 58 53 ; E-mail : catherine.passirani@univ-angers.fr ; Internet : www.u646.angers.inserm.fr

Abstract

PURPOSE: Stealth nanoparticles are generally obtained after modifying their surface with hydrophilic polymers such as PEG. In this study we analysed the effect of a phospholipid (DG) or protein (BSA) inclusion in porous cationic polysaccharide (NP^+) on their physico-chemical structure and the effect on complement activation. METHODS: NP^+s were characterised in terms of size, zeta potential (ζ) and static light-scattering (SLS). Complement consumption was assessed in normal human serum (NHS) by measuring the residual haemolytic capacity of the complement system. RESULTS: DG-loading did not change their size or ζ whereas progressive BSA loading decreased lightly their ζ. An electrophoretic mobility analysis study showed the presence of 2 differently-charged sublayers at the NP^+ surface which are not affected by DG-loading. Complement system activation, studied via a CH50 test, was suppressed by DG- or BSA-loading. We also demonstrated that NP^+s could be loaded by a polyanionic molecule such as BSA, after their preliminary filling by a hydrophobic molecule such as DG. CONCLUSION: These nanoparticles are able to absorb large amounts of phospholipids or proteins without change in their size or zeta potential. Complement studies showed that stealth behaviour is observed when they are loaded and saturated either with anionic phospholipid or proteins.

Key words: Haemolytic CH50 test, phospholipid, protein, 'soft' electrophoresis, nanomedicine

1. Introduction

Although new types of drugs (oligonucleotides, peptides, proteins and new anticancer drugs) are produced daily, their final therapeutic relevance, including their specificity and safety, is largely dependent on their bioavailability and specific distribution. These drugs need to be protected from degradation in biological fluids before reaching their targets, and need to be transported to specific sites prior to release. Colloidal drug carriers such as nanoparticles (NPs) or liposomes are expected to fulfil these requirements (1, 2). The main route for a large biodistribution of colloidal drug carriers remains intravenous (*i.v.)* administration (3). Unfortunately, many colloidal drug carriers undergo rapid elimination from the bloodstream and cannot be injected. The reason of this elimination is their recognition by the mononuclear phagocytic system (MPS) (4). This recognition is enhanced by blood-protein adsorption (opsonisation) and, in particular, by the presence of proteins of the complement system (5). Interactions between opsonins and colloidal drug carriers can be evaluated by several tests, such as the haemolytic CH50 test (6, 7). A greater understanding of complement-system protein interactions with particles has allowed the development of different strategies to reduce opsonisation. Normally, without opsonins that are bound or adsorbed on the particle surface, phagocytes are not able to bind or recognise foreign particles. Indeed, some nanoparticles are able to circulate for several hours; up to 45h in mice, rats and humans (8-10). In this case, NPs would have more chance to find their target or to benefit from the Enhanced Permeability and Retention effect (EPR effect), which is a specific characteristic of solid tumour (11, 12). The most common strategy is to modify the nanoparticle surface to create a displayed steric barrier, hence impeding protein adsorption (*e.g.* polyethylene glycol (PEG), heparin, dextran etc.). For this reason, most nanoparticles include PEG polymers in

their formulation in order to decrease complement system activation and macrophage uptake (13).

A drug delivery system based on synthetic polysaccharide nanoparticles has recently been developed (14). These nanoparticles are made of maltodextrin residues reticulated with epichlorhydrin. They can also be grafted with cationic ligands (NP^+s). Anionic molecules, such as dipalmitoyl phosphatidyl glycerol (DG) can be inserted inside their structure ($DGNP^+$)(15). They have been used as a delivery system for proteins, or lipophilic drugs inserted in the phospholipid core (15-18). These NPs have also been used by intranasal administration to increase the antinociceptive activity of nasal morphine in mice (19). After sub-lingual administration these cationic nanoparticles loaded with ovalbumin enhanced an induction of tolerance on an asthma model (20). Recently these neutral and cationic nanoparticles have also been shown to cross an *in vitro* model of the blood brain barrier (14, 21). In the present work, we characterised these cationic nanoparticles in terms of anionic model drug-loading (lipid or protein), surface charge study and complement protein activation.

2. Materials and methods

2.1. Materials

Maltodextrin (Glucidex®) was purchased from Roquette (France) and 1,2-dipalmitoyl-sn-glycero-3-phosphatidylglycerol (DG) from Lipoid® (Germany).

1-chloro-2,3-epoxypropan (epichlorhydrin) and glycidyltrimethylammonium chloride (hydroxycholine) came from Fluka (Saint-Quentin-Fallavier, France) and bovine serum albumin (BSA) came from Sigma (Steinheim, Germany). Normal human serum (NHS) was

provided by the *Etablissement Français du Sang* (Angers, France) and rabbit, anti-sheep, erythrocyte antibodies were supplied by Biomérieux (Sérum hémolytique, Biomérieux, France). NaCl was obtained from Prolabo (Fontenay-sous-Bois, France). Deionized water was obtained from a Milli-Q plus R system (Millipore, Paris, France) and saturated with N_2. The specific conductivity ($18.2 m\Omega.cm^{-1}$) and the surface tension ($72 mN.m^{-1}$) of this quality of water indicated that it was free of surface-active impurities.

2.2. Preparating, loading and labelling nanoparticles

Polysaccharide particles were prepared from US Pharmacopoeia maltodextrin, as described previously (15, 22). Briefly, 100g of maltodextrin was dissolved in 2N sodium hydroxide with magnetic stirring at room temperature. Further, 1-chloro-2,3-epoxypropane (epichlorhydrin), or a mixture of epichlorhydrin and glycidyl-trimethylammonium chloride (hydroxycholine, cationic ligand) was added to make neutral and cationic polysaccharide gels, respectively. The gels were then neutralised with acetic acid and sheared under high pressure in a Minilab homogenisor (Rannie; APV Baker, Evreux, France). The 60nm neutral and cationic polysaccharide nanoparticles (NP^0s and NP^+s respectively) obtained were ultra-filtered on an SGI Hi-flow system (hollow fibre module: 30 UFIB/1 S.6/40 kDa; Setric Génie Industriel, Toulouse, France) to remove low-molecular weight reagents and salts.

Porous cationic nanoparticles (NP^+s) into which anionic phospholipids were loaded ($DGNP^+$), were prepared according to Loiseau *et al.* by mixing at 60°C polysaccharide nanoparticles and ethanolic DG for 1 hour at different DG/cationic nanoparticle ratios (w/w) (10%, 30%, 50% and 70%), named $_{10,\ 30,\ 50}$ or $_{70}DGNP^+$s (15). The addition of DG was performed at a temperature above the gel-to-liquid phase transition temperature of the phospholipid (23).

BSA-loaded nanoparticles ($BSANP^+$s and $BSA/_{70}DGNP^+$s) were made by mixing NP^+s or $_{70}DGNP^+$s at 20°C for 10 min. with increasing amounts of BSA at different BSA / NPs ratios (w/w) (100%, 200%, 300%), named $_{100,\ 200}$ or $_{300}BSANP^+$s and $_{100}$ or $_{200}BSA/_{70}DGNP^+$s. After that, NPs were dialysed and packaged after a 0.2µm filtration.

The binding of BSA or DG to the NPs was evaluated using gel permeation chromatography on Sephadex and was found to be total. Biacore studies confirmed these results (24). Stability studies also showed that even after five days no protein was released from the NPs. $DGNP^+$ samples of over a year in solution were found to be stable in term of size, zeta potential and lipid insertion (data not shown).

2.3. Size and zeta potential determination

The average hydrodynamic diameter and the polydispersity index of nanoparticles were determined by dynamic light scattering using a Malvern Autosizer 4700 (Malvern Instruments S.A., Worcestershire, UK) fitted with a 488nm laser beam at a fixed angle of 90°. Measurements were taken at 25°C, with $0.89x10^{-2}$Pa.s viscosity and a refractive index of 1.33. The nanoparticles were concentrated at 0.5mg/ml in 15mM NaCl solution, to enable measurements (performed in triplicate), in order to assure a convenient scatter intensity on the detectors. The zeta potential measurements were carried out using a Zeta Sizer 2000 (Malvern Instruments, France) equipped with an AZ-4 cell and were based on the laser-doppler effect. Each sample was properly diluted with 15mM NaCl solution, in order to maintain the number of counts per second to around 600. Three measurements were carried out for each sample and mean values with standard deviations were calculated.

2.4. Static Light Scattering (SLS)

Molecular weight measurements were determined by SLS using a Malvern Autosizer 4700 (Malvern Instruments S.A., Worcestershire, UK) fitted with a 488nm laser beam at a fixed angle of 90°. Measurements used sample time-averaged intensity on a long time-scale relative to molecular diffusion (seconds to minutes) to determine the molecular weight (Mw) (in the typical range of 1kDa to 20MDa) (25, 26). They were taken at 25°C, with 0.89×10^{-2} Pa.s viscosity and a refractive index of 1.33. The nanoparticles were concentrated at 0.5 mg/ml in deionised water.

2.5. Electrophoretic mobility measurements

Electrophoretic mobility ($\boldsymbol{\mu}$) ($m^2.s^{-1}.V^{-1}$) measurements of NP^+s and $_{70}DGNP^+$s (particle speed in a given electric field) were performed using a Malvern Zeta Sizer 2000. Measurements were made as a function of NaCl concentrations in water at 25°C, with a dielectric constant of 79, a refractive index of 1.33, viscosity of 0.89×10^{-2}Pa.s, cell voltage of 150V, and a current of 5mA. The nanoparticles were diluted in Milli-Q water and different NaCl concentrations were used: 1.5, 2, 10 and 50mM. Each particle sample was diluted at the concentration of 1.16mg of NP/ml in Milli-Q water and the conductivity was measured at room temperature. Nanoparticle electrokinetic characteristics were determined using 'soft' particle electrophoresis analysis, as described by Ohshima (27), representing the best curve fitting the two-layer model. Analysis was carried out as described previously (28).

2.6. Transmission Electron Microscopy (T.E.M.) of nanoparticles

Electron microscopy images were obtained on a JEOL JEM2010 TEM. The direct observation of $_{70}$DGNP^{+}s was carried out by placing 10µL of $_{70}$DGNP^{+} solution onto a copper grid with a porous carbon film. The copper grid was placed on a piece of filter paper, so that buffer solution could be removed by filter paper. Negative staining was obtained by placing 10µL of 7 % uranyl acetate solution onto a sample grid for 5 minutes. Excess liquid was then removed from the sample by lightly touching the edge of filter paper with the edge of the grid. The sample grids were put in a desiccator overnight before the T.E.M. examination took place.

2.7. Complement activation

Complement consumption was assessed in normal human serum (NHS) by measuring the residual haemolytic capacity of the complement system after contact with NP^{0}s, NP^{+}s, $_{10, 30, 50}$ and $_{70}$DGNP^{+}s or $_{100, 200}$ and $_{300}$BSANP^{+}s. The technique consisted in determining the amount of serum required to haemolyse 50 % of a fixed number of sensitised sheep erythrocytes (CH50 units). A veronal-buffer saline containing 0.15mM Ca^{2+} and 0.5mM Mg^{2+} was prepared as previously described (VBS^{++}) (7). Sheep erythrocytes were sensitised by rabbit anti-sheep erythrocyte antibodies and suspended at a final concentration of 1.10^{8}cells/ml in VBS^{++}. To assess the consumption of CH50 units in the presence of the particles during a constant incubation time, increasing amounts of particle suspensions were added to NHS diluted in VBS^{++} so that the final dilution of NHS in the reaction mixture was ¼ (V/V) in a final volume of 1ml. After 60 minutes of incubation at 37°C with gentle agitation, the suspension was diluted at 1/25 (V/V) in VBS^{++} then aliquots at different dilutions were added

to a given volume of sensitised sheep erythrocytes. After 45 minutes of incubation at 37°C, the reaction mixture was centrifuged at 2,000rpm for 10 minutes. The absorption of the supernatant was determined at 415nm with a microplate reader (Multiskan Anscent, Labsystems SA, Cergy-Pontoise, France) and compared to the results obtained with the control serum. After determining the CH50 units remaining in the serum, the results were expressed as the consumption of CH50 units as a function of the nanoparticle surface area calculated as described elsewhere (28) in order to compare nanoparticles of different average diameters.

3. Results and discussion

3.1. Characterisation of DG or BSA insertion in NP^+s

Table 1 shows the mean hydrodynamic diameter, size distribution and zeta potential (ζ) of free NP or NP loaded with DG or BSA. We observed that neutral and cationic NPs had the same mean size and that DG-loading did not change the cationic NP size. Neutral nanoparticles (NP^0) had, as expected, a zeta potential of 0mV. All cationic NPs had a zeta potential around 30mV, even when they were prepared with increasing amounts of DG. No free liposomes were observed since DG liposomes prepared using the same conditions had a mean diameter of 250nm and a zeta potential of -41.5mV as previously described (29). Taken together, these results suggest that the anionic lipids strongly interact with the cationic NPs and penetrate totally within their structure. Indeed DG is an anionic lipid that can strongly interact with the cationic charges of the porous NP^+s. Experimentally we were not able to prepare NP with higher amounts of DG, since irreversible aggregation occurred, suggesting that the NP core was saturated by an excess of anionic lipids. NP^+s could also absorb large

amounts of BSA (6.8nm, ζ = -5.6mV) without size modification (Table 1). With BSA, the zeta potential decreased progressively with the increase of BSA loading. So, as for DG inclusion, no free BSA was observed, suggesting a total encapsulation of BSA.

DG insertion did not inhibit the additional insertion of BSA in $DGNP^+$s (Table 1). Saturation of the loading of the nanoparticles with BSA was faster in $DGNP^+$s compared to NP^+s (Fig. 1). Maximum BSA incorporation in $_{70}DGNP^+$s was 200% (w/w, protein/NP). BSA loading in NPs was confirmed by zeta potential and size analysis. BSA incorporation did not change DGNP sizes (Table 1). No additional peaks or polydispersity index rises were observed, indicating that no free proteins were detected. A decrease of zeta potential was observed when BSA incorporation exceeded 200% for NP^+s and 100% for $_{70}DGNP^+$s (Fig. 1). These results confirmed that the DG is inside the NP^+ core, limiting BSA loading, owing to the saturation of the NP^+ core by DG. The zeta potential decrease reflects the BSA progression from the inside toward the NP^+ surface as the core is progressively saturated (Fig. 1). The negative influence of BSA became more pronounced in $DGNP^+$s than NP^+s. Thus $_{200}BSA/_{70}DGNP^+$s had a neutral zeta potential. We observed that zeta potential standard deviation of free NP^+s is high while this standard deviation is lowered when lipids or proteins are absorbed. This result could be explained by the high mobility of the oligosaccharides on the surface of the nanoparticles where they are not filled by lipids or proteins. The absorption of anionic compounds should impair this surface mobility by structuring the inner part of the nanoparticles therefore lowering these movements and surface charge density.

3.2. T.E.M of nanoparticles and molecular weight determination

The $_{70}$DGNP^{+}s were observed by negative staining via T.E.M, in contrast to NP^{+}s and NP^{0}s (Fig. 2). These experiments, supported by observations made by De Miguel *et al*., indicated that NP might collapse due to dehydration and that its porous polysaccharide matrix was not dense enough for electron transmission (30).

The static light scattering measurement revealed an approximate Molecular weight of 4,000kDa for unloaded NP^{+}s which increased up to 11,000 kDa after post insertion of DG for $_{70}$DGNP^{+}s. Finally, T.E.M. observation, size and SLS measurements and zeta potential variations provided evidence that DG is indeed located inside the NP^{+}s.

3.3. Interfacial structure of NP predicted from 'soft' particle electrophoresis analysis

Electrophoretic mobility (***μ***) represents the velocity of a particle in a given electric field and its value is often converted into zeta potential value. 'Soft' particle electrophoresis analysis has been put into practice to predict NP interfacial structures (31). 'Soft' particle electrophoresis analysis, as described by Ohshima, has shown that 'soft' particle ***μ*** depended on the volume charge density distribution in the polyelectrolyte layer, particle size and also on applied oscillating electric field frequency. It depended upon frictional forces exerted on liquid flow by polymer segments, in the polyelectrolyte layer (27).

'Soft' particle theory allowed Na^{+} and Cl^{-} penetrability studies in different accessible layers on the NP surface (32). This theory can be used when ***μ*** is influenced by only one sublayer (33) or when it is influenced by two sublayers (34). Theoretical values of ***μ*** were calculated via soft-particle electrophoresis analysis (28) and compared to experimental data (Fig. 3). Two sublayers were considered at the NP^{+} surface (Fig. 3): an outer-sublayer (sublayer 1) characterised by a charge density Q1 for ionised groups and a thickness d, and an inner-sublayer (sublayer 2) with a charge density Q2 (34). The parameter λ characterises the

degree of friction exerted on the liquid flow at the surface layer. The reciprocal of λ (1/ λ) has the dimension of a length and can be considered as a 'softness' parameter. Q1, Q2, 1/λ and d were determined by a curve-fitting procedure. NP^+s and $_{70}DGNP^+$s displayed comparable results. Identical values were found for best NP^+ and $_{70}DGNP^+$ curve-fitting analysis. This showed that their $\boldsymbol{\mu}$ might be dependent on two sublayers with different charges ($R^2 = 0.97$). The outer sublayer was found to have a Q1 = 2.40 $x10^6 C.m^{-3}$ and a thickness d = 2.99 $x10^{-9}$m. The inner-sublayer had a Q2 = 4.48 $x10^2 C.m^{-3}$ and these NPs had a 1/λ = 4.00 $x10^{-9}$m (Table 2). Despite the incorporation of high amounts of DG in NP^+s, these NPs presented no significant difference in their surface charge accessibility. The presence of these two sublayers might be surprising, especially because cationic groups are grafted homogeneously during the synthesis of the NP^+ gel. This could be explained by the hypothesis of the presence of a counter-ion gradient (Fig. 4). During nanoparticle synthesis, cationic groups provided by a quaternary ammonium graft ($RN\text{-}(CH_3)_3^+$), were associated with anionic counter ions. During the last step of nanoparticle synthesis, most of the counter ions were eliminated by ultrafiltration in Milli-Q water.

The BSA and DG incorporation into $_{70}DGNP^+$s and $_{100}$ and $_{200}BSANP^+$s did not modify the size, the zeta potential nor the electrophoretic mobility curves. This might suggest that DG and BSA are internalised too deeply inside the NP^+ core to influence its $\boldsymbol{\mu}$ and consequently the ζ. This is not the case for high amounts of BSA and for NP^+s already filled with DG and secondly filled with BSA (Table 1).

3.4. Complement activation

Opsonisation is the process whereby foreign organisms or particles become covered with opsonin proteins, thereby making them more visible to phagocytic cells. The capacity of NPs

to bind opsonin proteins can be appreciated by different assays, one of them being the haemolytic CH50 test. This test can be considered as an *in vitro* indicator before intravenous (i.v.) administration in animals (35). The CH50 test consists in measuring the haemolytic activity of a human serum versus 50% of sheep erythrocyte concentration remaining after contact with particles (6, 7, 36). The consumption of CH50 units is measured at a fixed amount of human serum (HS) in the presence of an increasing surface area of particles.

As shown in Fig. 5, CH50 unit consumption for cationic NP^+s without any DG or BSA was tested and was shown to be a strong activator of the complement system: 100% activation was obtained for 100cm^2/ml of NP^+ surface area. This is equivalent to what has already been observed with synthetic poly (methyl methacrylate) NPs which were found to have a half-life of only 3 minutes in mice plasma circulation (37). Two factors could be involved in this high level of activation. The first is the high cationic charge at the NP^+ surface. The literature has described that charged particles, particularly cationic ones, are generally strong activators of the immune system (38, 39). Any of several attractive forces including Van der Walls, electrostatic, ionic and hydrogen bonds can be involved in opsonin binding to the NP^+ surface (40). The second is the presence of a polysaccharide backbone including many hydroxyl (OH) groups. Indeed, the complement proteins C3b were known to bind on dextran particle surfaces thanks to polysaccharidic OH groups (41, 42). They result from complement proteins C3 cleavage which makes the internal thioester bond available to react with OH groups. Thioester bond was formerly located inside a hydrophobic pocket (43) and makes visible thanks to the C3 cleavage. This high level of interaction with the complement protein C3b can trigger alternative pathways of complement system activity (44). A nucleophilic link between OH groups and C3b thioester bonds depends on OH electronic density, but also on the polymer backbone type and polymer conformation (44). This can explain dextran ability to decrease complement activation depending on their brush or mushroom conformation at NP surfaces

(37). However NP^0s, which are made with the same polysaccharide backbone, did not activate the complement system, even at 250cm^2/ml (Fig. 5a), in accordance with the literature (3, 45). We can conclude that this polymer backbone is not a complement activator despite the presence of OH groups and that ionic interactions of NP^+s play a key role in the complement activation of these porous nanoparticles.

40% activation was obtained for 22cm^2/ml for DG liposomes. These liposomes are rather rigid with a negative charge at their surface (Fig. 5a) (29, 46). These two parameters are often associated with high levels of complement activation. However, contrary to what might be expected, DG incorporation inside NP^+s decreased CH50 unit consumption. Nanoparticles containing 10% of DG were still strong activators (Fig. 5a). When DG percentage was increased to 30%, no activation was observed for the same surface area. 100% activation was obtained at around 180cm^2. A strong decrease of CH50 consumption units was correlated to an increase of DG content with a dramatic effect observed when nanoparticles contained 50% or 70% of DG. Indeed 100% activation was reached for a 222cm^2/ml for $_{50}$DGNP^+s and $_{70}$DGNP^+s even at 250cm^2/ml did not activate the complement system (Fig. 5a).

To evaluate if the decrease of complement activation was due to the filling of the NP^+ frame by any component, or especially by the hydrophobic component, we assessed CH50 consumption units for hydrophilic molecule (BSA)-loaded NP^+s. Free BSA did not activate the complement system even at 250cm^2/ml. $_{100}$BSANP^+s were also strong activator with 90% activation obtained for a 125cm^2 nanoparticle surface area (Fig. 5b). When BSA incorporation increased to 200% and 300% a large decrease in CH50 unit consumption was observed. Indeed, the maximum level of activation for $_{200}$BSANP^+s and for $_{300}$BSANP^+s was only of 20% at 190 and 250cm^2/ml of particles, respectively (Fig. 5b). These results demonstrated that filling the NP^+ frame with high amounts of anionic model drugs, BSA or DG in our case, led

to stopping the activation of the complement system, whereas BSA- and DG-loading did not cancel the zeta potential of NP^+s.

In contrast to BSA, it seems that opsonins might not be loaded in $_{70}$DGNP^+s because of their high molecular weight (over 150kDa) (5, 47). Porous parts of NP^+ not filled by DG might be too small to contain opsonins.

Our study showed an inhibition of complement activation by BSA or DG loading inside NP^+ which might be compared to inhibition obtained after long chain of poly(ethylene glycol) (PEG) addition to strong activator nanoparticles, as shown by Van Butsele et al., Aqil et al. and Layer et al. (48-51). Indeed PEG create a steric barrier around particles able to protect against protein adsorption due to a decrease of surface hydrophobicity and a neutralization of surface potential. However high BSA or high DG loading inside NP^+ inhibit the complement activation as much as PEG addition on poly (methylmethacrylate-co-methacrylic acid) nanoparticle surface (52), but without cancelling the surface potential of these nanoparticles.

4. Conclusion

These studies performed on cationic nanoparticles have demonstrated that they behave as sponges able to absorb high amounts of BSA and DG. This absorption changed neither their surface nor their size up to a certain amount. The incorporation of DG was characterised by an increase of NP molecular weight analysed by static light scattering. Studies performed on complement protein consumption showed that DG insertion progressively lowers the amount of complement proteins adsorbed up to a level of total inhibition. We have also demonstrated that NP^+s can be loaded by a polyanionic molecule such as BSA despite their preliminary filling by a hydrophobic molecule such as DG. Thus these NPs could be considered as a

genuine co-delivery system. In contrast to other nanostructured systems (8, 9, 37) in our case, the loaded drug itself was able to generate stealth NPs and represents an alternative to the use of PEG. We are currently studying the pharmacokinetics and biodistribution of these nanoparticles after *in vivo* administration and their potential as delivery system of a lipophilic drug

5. Acknowledgments

We would like to thank Myriam Moreau, Christina Hubert (Inserm U646) and Pierre Legras (Animalerie Hospitalo-Universitaire,CHU, Angers, France) for technical support as well as Dr Alain Chevalier (Laboratoire d'Immunologie et Allergologie, Espace Centre Hospitalio-Universitaire d'Angers) for normal human serum supplies. We would like also to thank Robert Filmon and Romain Mallet from the *Service Commun d'Imagerie et d'Analyses Microscopiques* and Michel Terray from Malvern Instruments. A. Paillard was supported by a grant from *Le comité départemental de la Ligue Contre le Cancer*. This work was also supported by the *Cancéropôle Grand-Ouest* and by *la Ligue National Contre le Cancer* via *Equipe Labellisée 2007* funding.

Bibliography

1. M. Morille, C. Passirani, A. Vonarbourg, A. Clavreul, and J. P. Benoit. Progress in developing cationic vectors for non-viral systemic gene therapy against cancer. *Biomaterials* **29**: 3477-96 (2008).
2. D. C. Drummond, C. O. Noble, M. E. Hayes, J. W. Park, and D. B. Kirpotin. Pharmacokinetics and in vivo drug release rates in liposomal nanocarrier development. *J Pharm Sci* **97**: 4696-740 (2008).
3. S. M. Moghimi, A. C. Hunter, and J. C. Murray. Long-circulating and target-specific nanoparticles: theory to practice. *Pharmacol Rev* **53**: 283-318 (2001).

4. C. Passiraniand J. P. Benoit. Complement activation by injectable colloidal drug carriers. In R. I. Mahato (ed), *Biomaterials for Delivery and Targeting of Proteins and Nucleic Acids* (R. I. Mahato, ed), New York: CRC, 2005, pp. 187-230.
5. H. J. Muller-Eberhard. Molecular Organization and Function of the Complement System. 321-343 (1988).
6. M. Mayer. Complement and Complement fixation. In Kabat EA, Mayer MM, eds. Experimental immunochemistry; énd edn. Springfield, IL, USA: Thomas. 133-156 (1961).
7. M. Kazatchkine, G. Hauptmann, and U. Nydegger. Techniques du Complement. *Livre ed.INSERM collection technique en immunologie* 22-33 (1986).
8. A. L. Klibanov, K. Maruyama, V. P. Torchilin, and L. Huang. Amphipathic polyethyleneglycols effectively prolong the circulation time of liposomes. *FEBS Lett* **268**: 235-7 (1990).
9. T. M. Allenand A. Chonn. Large unilamellar liposomes with low uptake into the reticuloendothelial system. *FEBS Lett* **223**: 42-6 (1987).
10. A. Gabizon, R. Isacson, E. Libson, B. Kaufman, B. Uziely, R. Catane, C. G. Ben-Dor, E. Rabello, Y. Cass, T. Peretz, A. Sulkes, R. Chisin, and Y. Barenholz. Clinical studies of liposome-encapsulated doxorubicin. *Acta Oncologica* **33**: 779-786 (1994).
11. H. Maeda, J. Wu, T. Sawa, Y. Matsumura, and K. Hori. Tumor vascular permeability and the EPR effect in macromolecular therapeutics: a review. *J Control Release* **65**: 271-84 (2000).
12. Y. Matsumuraand H. Maeda. A new concept for macromolecular therapeutics in cancer chemotherapy: mechanism of tumoritropic accumulation of proteins and the antitumor agent smancs. *Cancer Res* **46**: 6387-92 (1986).
13. A. Vonarbourg, C. Passirani, P. Saulnier, P. Simard, J. C. Leroux, and J. P. Benoit. Evaluation of pegylated lipid nanocapsules versus complement system activation and macrophage uptake. *J Biomed Mater Res A* **78**: 620-8 (2006).
14. Y. Jallouli, A. Paillard, J. Chang, E. Sevin, and D. Betbeder. Influence of surface charge and inner composition of porous nanoparticles to cross blood-brain barrier in vitro. *Int J Pharm* **344**: 103-9 (2007).
15. P. M. Loiseau, L. Imbertie, C. Bories, D. Betbeder, and I. De Miguel. Design and antileishmanial activity of amphotericin B-loaded stable ionic amphiphile biovector formulations. *Antimicrob Agents Chemother* **46**: 1597-601 (2002).
16. A. Debin, R. Kravtzoff, J. V. Santiago, L. Cazales, S. Sperandio, K. Melber, Z. Janowicz, D. Betbeder, and M. Moynier. Intranasal immunization with recombinant antigens associated with new cationic particles induces strong mucosal as well as systemic antibody and CTL responses. *Vaccine* **20**: 2752-63 (2002).
17. S. El mir, A. Casanova, D. Betbeder, and F. Triebel. A combination of interleukin-2 and 60 nm cationic supramolecular biovectors for the treatment of established tumours by subcutaneous or intranasal administration. *Eur J Cancer* **37**: 1053-60 (2001).
18. B. C. Baudner, O. Balland, M. M. Giuliani, P. Von Hoegen, R. Rappuoli, D. Betbeder, and G. Del Giudice. Enhancement of protective efficacy following intranasal immunization with vaccine plus a nontoxic LTK63 mutant delivered with nanoparticles. *Infect Immun* **70**: 4785-90 (2002).
19. D. Betbeder, S. Sperandio, J. P. Latapie, J. de Nadai, A. Etienne, J. M. Zajac, and B. Frances. Biovector nanoparticles improve antinociceptive efficacy of nasal morphine. *Pharm Res* **17**: 743-8 (2000).
20. A. Razafindratsita, N. Saint-Lu, L. Mascarell, N. Berjont, T. Bardon, D. Betbeder, L. Van Overtvelt, and P. Moingeon. Improvement of sublingual immunotherapy efficacy

with a mucoadhesive allergen formulation. *J Allergy Clin Immunol* **120**: 278-85 (2007).
21. L. Fenart, A. Casanova, B. Dehouck, C. Duhem, S. Slupek, R. Cecchelli, and D. Betbeder. Evaluation of effect of charge and lipid coating on ability of 60-nm nanoparticles to cross an in vitro model of the blood-brain barrier. *J Pharmacol Exp Ther* **291**: 1017-22 (1999).
22. M. Major, E. Prieur, J. F. Tocanne, D. Betbeder, and A. M. Sautereau. Characterization and phase behaviour of phospholipid bilayers adsorbed on spherical polysaccharidic nanoparticles. *Biochim Biophys Acta* **1327**: 32-40 (1997).
23. M. C. Woodleand D. Papahadjopoulos. Liposome preparation and size characterization. *Methods Enzymol* **171**: 193-217 (1989).
24. J. P. Siguier, M. Major, and O. Balland. Development of a new method to characterize (SMBV) antigen formulations using surface plasmon resonance technology. *Int J Pharm* **242**: 411-5 (2002).
25. M. M. Domingues, P. S. Santiago, M. A. R. B. Castanho, and N. C. Santos. What can light scattering spectroscopy do for membrane-active peptide studies? *Journal of Peptide Science* **14**: 394-400 (2008).
26. E. Serefoglou, J. Oberdisse, and G. Staikos. Characterization of the soluble nanoparticles formed through coulombic interaction of bovine serum albumin with anionic graft copolymers at low pH. *Biomacromolecules* **8**: 1195-1199 (2007).
27. H. Ohshima. Electrokinetics of soft particles. *Colloid & Polymer Science* **285**: 1411-1421 (2007).
28. A. Vonarbourg, P. Saulnier, C. Passirani, and J. P. Benoit. Electrokinetic properties of noncharged lipid nanocapsules: influence of the dipolar distribution at the interface. *Electrophoresis* **26**: 2066-75 (2005).
29. K. Matsuzaki, M. Harada, S. Funakoshi, N. Fujii, and K. Miyajima. Physicochemical determinants for the interactions of magainins 1 and 2 with acidic lipid bilayers. *Biochim Biophys Acta* **1063**: 162-70 (1991).
30. I. De Miguel, L. Imbertie, V. Rieumajou, M. Major, R. Kravtzoff, and D. Betbeder. Proofs of the structure of lipid coated nanoparticles (SMBV) used as drug carriers. *Pharm Res* **17**: 817-24 (2000).
31. H. Ohshima. Electrophoretic Mobility of Soft Particles. *Journal of Colloid and Interface Science* **163**: 474-483 (1994).
32. V. Ducel, P. Saulnier, J. Richard, and F. Boury. Plant protein-polysaccharide interactions in solutions: application of soft particle analysis and light scattering measurements. *Colloids Surf B Biointerfaces* **41**: 95-102 (2005).
33. K. Makino, N. Yamamoto, K. Higuchi, N. Harada, H. Ohshima, and H. Terada. Phagocytic uptake of polystyrene microspheres by alveolar macrophages: effects of the size and surface properties of the microspheres. *Colloids and Surfaces B: Biointerfaces* **27**: 33-39 (2003).
34. K. Makino, M. Umetsu, Y. Goto, A. Nakayama, T. Suhara, J. Tsujii, A. Kikuchi, H. Ohshima, Y. Sakurai, and T. Okano. Interaction between charged soft microcapsules and red blood cells: effects of PEGylation of microcapsule membranes upon their surface properties. *Colloids and Surfaces B: Biointerfaces* **13**: 287-297 (1999).
35. A. Beduneau, P. Saulnier, N. Anton, F. Hindre, C. Passirani, H. Rajerison, N. Noiret, and J. P. Benoit. Pegylated nanocapsules produced by an organic solvent-free method: Evaluation of their stealth properties. *Pharm Res* **23**: 2190-9 (2006).
36. D. Labarre, B. Montdargent, M. Carreno, and F. Maillet. Strategy for in vitro evaluation of the interactions between biomaterials and complement system. *Journal of Applied Biomaterials* **4**: 231-240 (1993).

37. C. Passirani, G. Barratt, J. P. Devissaguet, and D. Labarre. Long-circulating nanoparticles bearing heparin or dextran covalently bound to poly(methyl methacrylate). *Pharm Res* **15**: 1046-50 (1998).
38. M. Roser, D. Fischer, and T. Kissel. Surface-modified biodegradable albumin nano- and microspheres. II: effect of surface charges on in vitro phagocytosis and biodistribution in rats. *Eur J Pharm Biopharm* **46**: 255-63 (1998).
39. A. Vonarbourg, C. Passirani, P. Saulnier, and J. P. Benoit. Parameters influencing the stealthiness of colloidal drug delivery systems. *Biomaterials* **27**: 4356-73 (2006).
40. C. D. Blackand G. Gregoriadis. Interaction of liposomes with blood plasma proteins. *Biochem Soc Trans* **4**: 253-6 (1976).
41. J. Toufikand D. Labarre. Relationship between reduction of complement activation by polysaccharide surfaces bearing diethylaminoethyl groups and their degree of substitution. *Biomaterials* **16**: 1081-8 (1995).
42. M. P. Carreno, D. Labarre, M. Jozefowicz, and M. D. Kazatchkine. The ability of Sephadex to activate human complement is suppressed in specifically substituted functional Sephadex derivatives. *Mol Immunol* **25**: 165-71 (1988).
43. S. K. Law, T. M. Minich, and R. P. Levine. Binding reaction between the third human complement protein and small molecules. *Biochemistry* **20**: 7457-63 (1981).
44. D. Labarre, A. Laurent, A. Lautier, S. Bouhni, L. Kerbellec, J. M. Lewest, and N. Tersinet. Complement activation by substituted polyacrylamide hydrogels for embolisation and implantation. *Biomaterials* **23**: 2319-27 (2002).
45. D. E. Owens, 3rdand N. A. Peppas. Opsonization, biodistribution, and pharmacokinetics of polymeric nanoparticles. *Int J Pharm* **307**: 93-102 (2006).
46. A. Gabizonand D. Papahadjopoulos. The role of surface charge and hydrophilic groups on liposome clearance in vivo. *Biochim Biophys Acta* **1103**: 94-100 (1992).
47. C. L. Villiers, M. B. Villiers, and P. N. Marche. [Role of the complement C3 protein in the control of the specific immune response]. *Ann Biol Clin (Paris)* **57**: 127-35 (1999).
48. A. Aqil, S. Vasseur, E. Duguet, C. Passirani, J. P. Benoît, A. Roch, R. Müller, R. Jérôme, and C. Jérôme. PEO coated magnetic nanoparticles for biomedical application. *European Polymer Journal* **44**: 3191-3199 (2008).
49. K. V. Butsele, S. Cajot, S. V. Vlierberghe, P. Dubruel, C. Passirani, J.-P. Benoit, R. Jérôme, and C. Jérôme. pH-Responsive Flower-Type Micelles Formed by a Biotinylated Poly(2-vinylpyridine)-block-poly(ethylene oxide)-block-poly(E-caprolactone) Triblock Copolymer. *Advanced Functional Materials* **19**: 1416-1425 (2009).
50. K. Van Butsele, P. Sibret, C. A. Fustin, J. F. Gohy, C. Passirani, J. P. Benoit, R. Jerome, and C. Jerome. Synthesis and pH-dependent micellization of diblock copolymer mixtures. *J Colloid Interface Sci* **329**: 235-43 (2009).
51. A. Layre, P. Couvreur, H. Chacun, J. Richard, C. Passirani, D. Requier, J. P. Benoit, and R. Gref. Novel composite core-shell nanoparticles as busulfan carriers. *J Control Release* **111**: 271-80 (2006).
52. J. Rieger, C. Passirani, J.-P. Benoit, K. Van Butsele, R. Jérôme, and C. Jérôme. Synthesis of Amphiphilic Copolymers of Poly(ethylene oxide) and Poly(&egr;-caprolactone) with Different Architectures, and Their Role in the Preparation of Stealthy Nanoparticles. *Advanced Functional Materials* **16**: 1506-1514 (2006).

Table I

Physical characterisation of NP

Particle type	Mean diameter (nm)	p.i.	Zeta potential (mV)
DG Liposomes	250.0± 0.20	0.16	- 41.5 ± 5.70
Free BSA	6.80 ± 2.22	0.25	- 5.6 ± 1.9
NP^0	60.3 ± 3,11	0.25	0.1 ± 0.90
NP^+	63.1 ± 0,40	0.21	25.5 ± 17.50
$_{100}BSANP^+$	62.0 ± 0,30	0.17	20.8 ± 10.30
$_{200}BSANP^+$	61.1 ± 0.55	0.11	16.8 ± 8.47
$_{300}BSANP^+$	61.7 ± 0.23	0.17	12.1 ± 3.89
$_{10}DGNP^+$	58.4 ± 6.77	0.19	31.1 ± 1.92
$_{30}DGNP^+$	60.9 ± 1.64	0.14	29.9 ± 0.81
$_{50}DGNP^+$	60.2 ± 5.70	0.19	30.6 ± 0.90
$_{70}DGNP^+$	59.0 ± 3.60	0.20	30.6 ± 6.79
$_{100}BSA/_{70}DGNP^+$	61.7 ± 2.31	0.15	16.0 ± 4.94
$_{200}BSA/_{70}DGNP^+$	62.1 ± 3.72	0.23	2.16 ± 3.85

Mean diameters, polydispersity index (p.i.) and zeta potential values of NP^+, $_{10, 30, 50, 70}DGNP^+$, DG liposomes and free BSA. ± indicates the SD of experimentations.

ction in mice. AUC_{tot} (% dose/min.) : total area under the curve; $t_{1/2}$ (min.) : half-life time

Table II

Values of surface charge density, softness parameter and thickness of NP^+ and $_{70}DGNP^+$ interfacial structures

Particle	Q1 ($C.m^{-3}$)	Q2 ($C.m^{-3}$)	1/λ (m)	d (m)
Curve-fitting for NP^+ and $_{70}DGNP^+$	2.40×10^{6}	4.48×10^{2}	4.00×10^{-9}	2.99×10^{-9}

Q1, Q2, 1/λ and *d* parameters for NP^+ and $_{70}DGNP^+$ determined by the calculation of curve-fitting by using Ohshima's method. The correlation between the experimental and theoretical curves was determined for NP^+ and $_{70}DGNP^+$ (R^2= 0.97)

Legend to Figures

Figure 1

Zeta potential evolution for NP^+ and $_{70}DGNP^+$ with BSA increasing incorporation in the presence of 15mM NaCl. ***, $p < 0.01$ (Fisher's test)

Figure 2

Transmission electronic microscopy images of $_{70}DGNP^+$after uranyl acetate treatment; bar represents 50nm.

Figure 3

Evolution of electrophoretic mobility as a function of NaCl concentration at physiologic pH (7.4) for NP^+ (○) and $_{70}DGNP^+$ (◊). Theoretical curve fitting (**-**) was obtained from the equation described previously with ZN and 1/λ, chosen in order to fit as closely as possible the experimental curve.

Figure 4

Schematic representation of NP^+ internal organisation with two charged surface sublayers where d is the thickness of sublayer 1 and (ci) is the remaining counter ions

Figure 5

Consumption of CH50 units in the presence of single DPPG liposomes (▲), NP^0 (●), NP^+ (■), $_{10}$ (Δ), $_{30}$ (○), $_{50}$ (◊), (□) $_{70}DGNP^+$ (**A**). Consumption of CH50 units in the presence of single free BSA (●),NP^+ (■), $_{100}$ (Δ), $_{200}$ (◊), $_{300}$ (□) $BSANP^+$ (**B**).

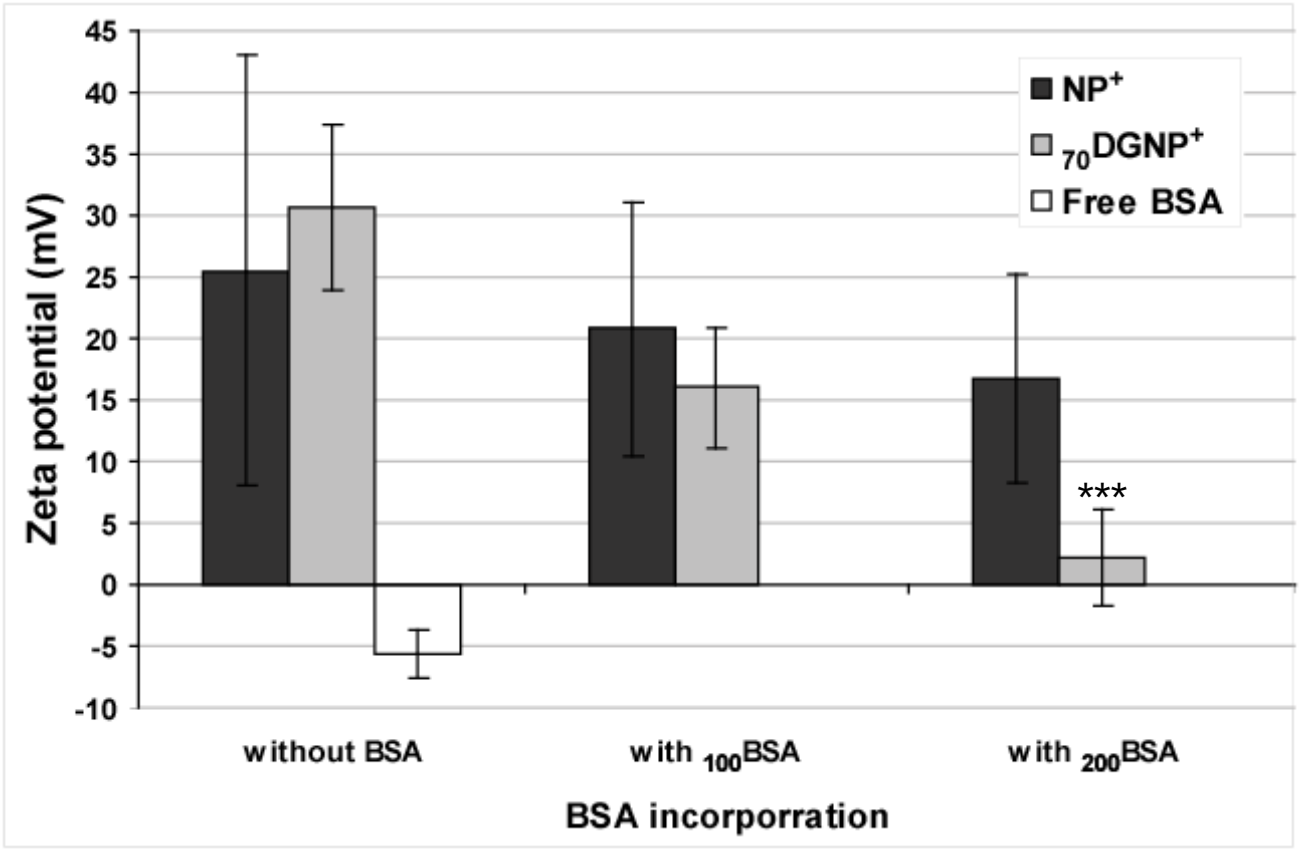

Figure 1

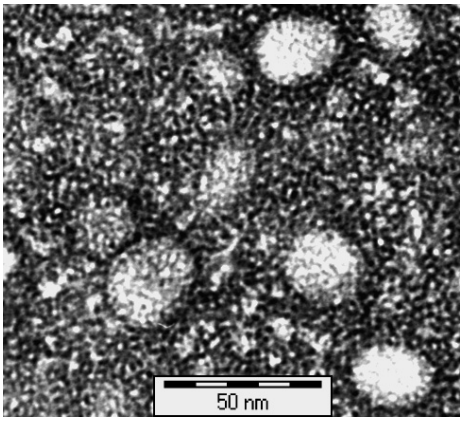

Figure 2

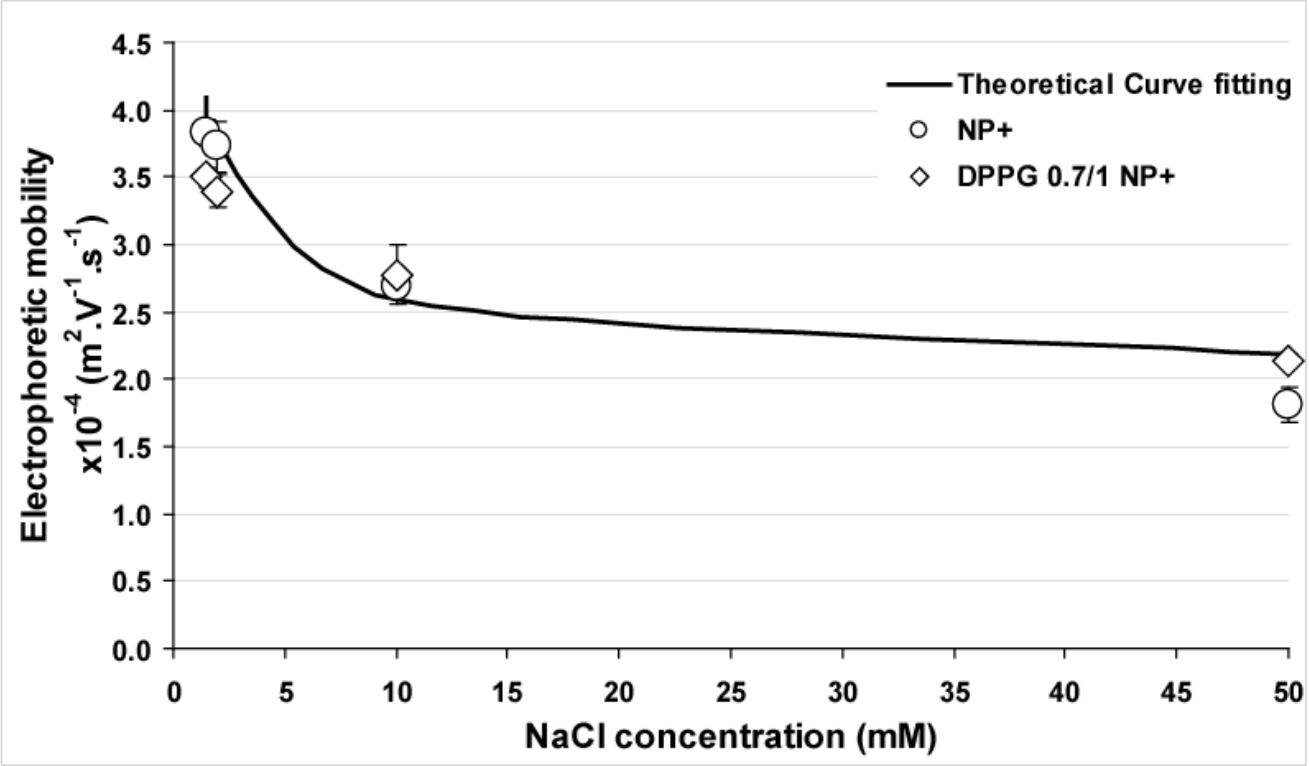

Figure 3

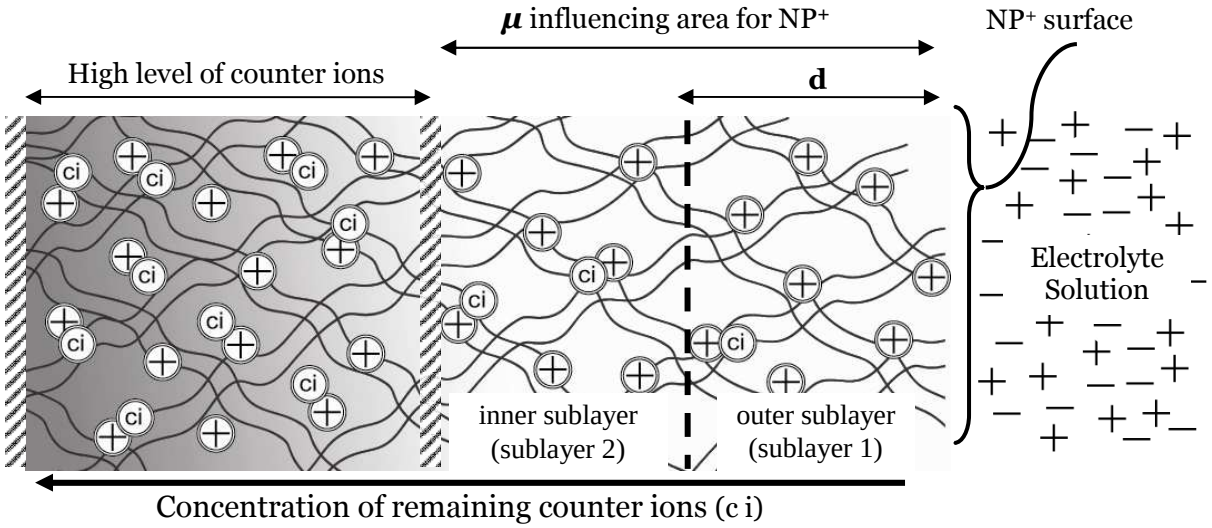

Figure 4

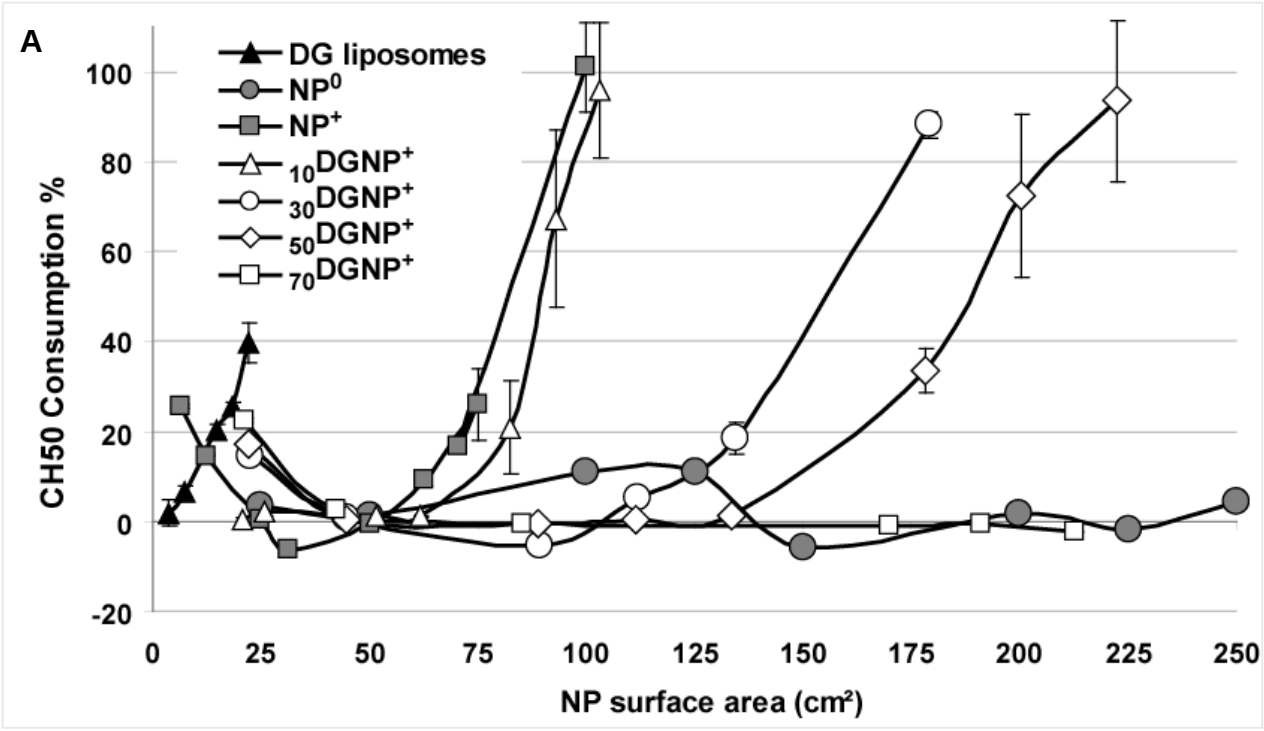
A
DG liposomes
NP0
NP+
10DGNP+
30DGNP+
50DGNP+
70DGNP+
CH50 Consumption %
NP surface area (cm²)

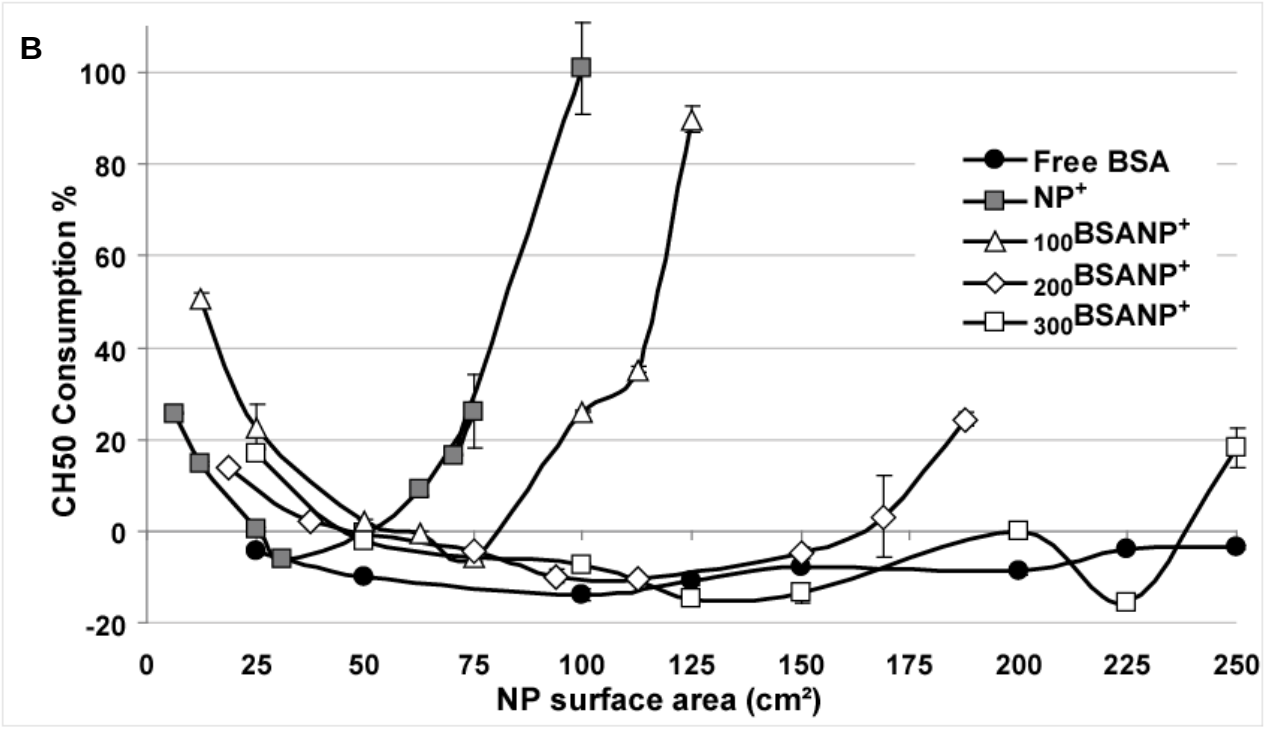
B
Free BSA
NP+
100BSANP+
200BSANP+
300BSANP+
CH50 Consumption %
NP surface area (cm²)

Figure 5